ACS NANO

www.acsnano.org

ARTICLE

Ganglioside-Functionalized Nanoparticles for Chimeric Antigen Receptor T-Cell Activation at the Immunological Synapse

Han Zang, Menna Siddiqui, Suryaram Gummuluru, Wilson W. Wong, and Björn M. Reinhard*

Cite This: https://doi.org/10.1021/acsnano.2c06516 Read Online

ACCESS | Metrics & More | Article Recommendations | Supporting Information

ABSTRACT: Chimeric Antigen Receptor (CAR) T cell therapy has proven to be an effective strategy against hematological malignancies but persistence and activity against solid tumors must be further improved. One emerging strategy for enhancing efficacy is based on directing CAR T cells to antigen presenting cells (APCs). Activation of CAR T cells at the immunological synapse (IS) formed between APC and T cell is thought to promote strong, persistent antigen-specific T cell-mediated immune responses but requires integration of CAR ligands into the APC/T-cell interface. Here, we demonstrate that CAR ligand functionalized, lipid-coated, biodegradable polymer nanoparticles (NPs) that contain the ganglioside GM3 (GM3-NPs) bind to CD169 (Siglec-1)-expressing APCs and localize to the cell contact site between APCs and CAR T cells upon initiation of cell conjugates. The CD169$^+$ APC/CAR T-cell interface is characterized by a strong optical colocalization of GM3-NPs and CARs, enrichment of F-actin, and recruitment of ZAP-70, indicative of integration of GM3-NPs into a functional IS. Ligands associated with GM3-NPs localized to the APC/T-cell contact site remain accessible to CARs and result in robust T-cell activation. Overall, this work identifies GM3-NPs as a potential antigen delivery platform for active targeting of CD169 expressing APCs and enhancement of CAR T-cell activation at the NP-containing IS.

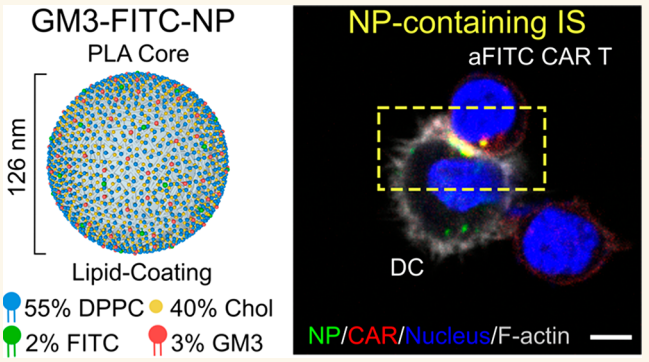

KEYWORDS: *biomimetic nanomaterials, lipid-coated polymeric nanoparticle, ganglioside GM3, Siglec-1/CD169, antigen presenting cell, CAR T cell activation*

Antigen-presenting cells (APCs) collect and process antigens and present them to T cells via major histocompatibility complexes (MHCs) at the immunological synapse (IS) formed between APC and T cell. The cell contact at the IS is critical for a successful priming of T cells and inducing a T cell-mediated immune response against a specific antigen. There has been considerable interest in devising strategies for recruiting T lymphocytes to target tumor associated antigens and to eradicate cancer cells. One strategy is based on engineered chimeric antigen receptors (CARs) that once transduced into CD8$^+$ T cells can initiate a highly specific cytotoxic response against cells expressing a targeted antigen. CAR T cell therapy has proven to be an effective strategy against hematological malignancies but still needs to improve persistence and activity against solid tumors.[1] Intriguingly, Irvine and co-workers[2] demonstrated that priming of CAR T cells through dendritic cells (DCs) in the lymph nodes, which is the native environment for T cell priming, is particularly effective in enhancing the efficacy of CAR T cells, including against solid tumors. Albumin was used as a vector to transport CAR ligands into mouse lymph nodes via the lymph flow after subcutaneous injection. The CAR ligands were covalently linked to the headgroup of phospholipids, which allowed these amphiphilic ligands ("amph-ligands") to transfer from albumin to cell membranes and to achieve CAR ligand presentation on APCs in lymph nodes. However, the amph-ligand strategy also has some limitations. Albumin lacks active targeting functionalities and, instead, relies exclusively on the structure of the lymph node to provide preferential interaction between APCs and amph-ligands that pass through the lymph node.

Received: July 2, 2022
Accepted: October 21, 2022

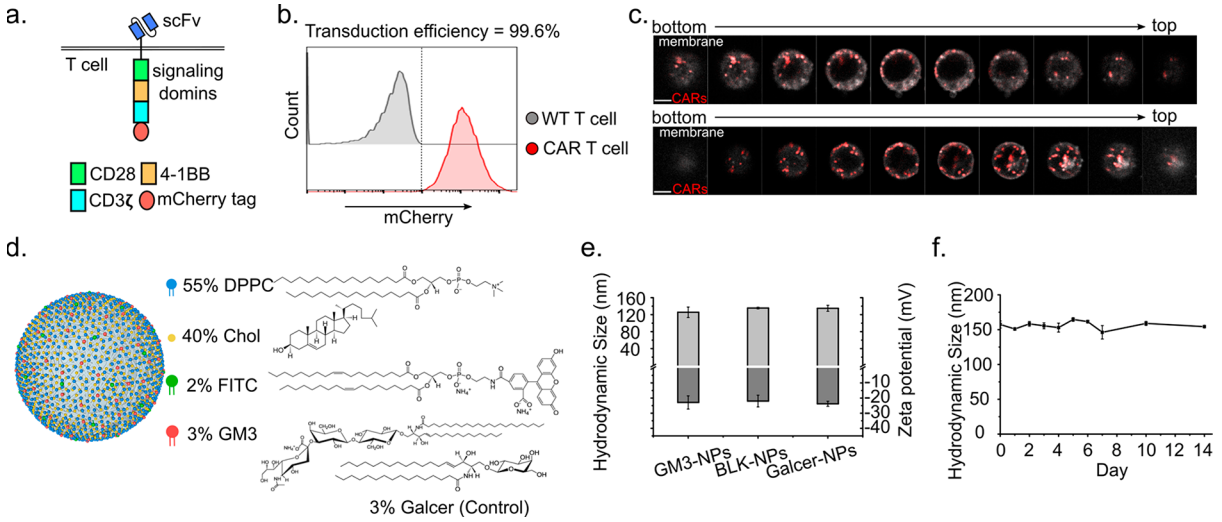

Figure 1. Design and characterization of GM3-FITC-NPs for αFITC Jurkat CAR T cell activation. (a) Scheme of αFITC CAR construct. The extracellular domain contains scFv and the intracellular domain comprises CD28, 4−1BB, and CD3ζ signaling domains. CAR is tagged with mCherry in the intracellular domain. (b) Representative flow cytometry histograms (mCherry fluorescence) from transfected αFITC Jurkat CAR T cell (red) and wild-type Jurkat T cell (gray). (c) Z-stack confocal sections of two αFITC Jurkat CAR T cells from bottom to top. Step size = 1 μm. Scale bar = 5 μm. (d) Scheme of GM3-FITC-NPs and molecular structures of the lipid components (DPPC, Chol, GM3, Galcer). (e) Hydrodynamic size and zeta potential of GM3-FITC-NPs, BLK-FITC-NPs (no gangliosides) and Galcer-FITC-NPs. (f) Hydrodynamic diameter of GM3-FITC-NPs in cell culture media at 37 °C measured over 2 weeks. Data in panels (e) and (f) represent average ± standard deviation (n = 3).

Furthermore, lipid trafficking and endocytosis limit the dwell time of lipid-associated ligands on the cell surface and complicate the establishment of prolonged CAR T-cell priming with amph-ligands. Lastly, delivery of ligands to the plasma membrane of APCs per se may not warrant their efficient integration into the IS that is formed at the interface between CAR T cell and APC where ligand−CAR binding and costimulatory interactions, for instance between CD80/CD86 and CD28, and enrichment of F-actin act together to achieve a strong and persistent CAR T-cell activation.[3−5]

Although the accumulation of CAR ligands in the IS is highly desirable for achieving optimized CAR T-cell activation, rational strategies for efficient and selective integration of CAR ligands into this important intercellular interface are currently lacking. Nanoparticles (NPs) have properties that make them an interesting platform for integrating CAR ligands into the IS.[6,7] NPs are sufficiently small to retain some mobility in the interstitial space but are large enough to avoid removal through nonfenestrated vascular capillaries and gain access to APCs via the lymphatic system.[8,9] Functionalization of these NPs with ligands that are recognized by APC receptors facilitates selective binding to APCs. CD169 (Siglec-1) is a receptor of particular interest, because it has high expression levels on subsets of macrophages and DCs in secondary lymphoid tissues.[10−13] CD169 recognizes the sialyllactose group of monosialodihosylganglioside (GM3). Although the binding affinity of free GM3 lipid is low (the dissociation constant K_d lies in the mM range[12,14]), multivalent presentation of GM3 on NPs enhances the binding avidity to CD169$^+$ macrophages and DCs. CD169-targeting liposome-based platforms have been utilized to deliver antigen and toll-like receptor (TLR) agonists to CD169$^+$ APCs and enhance T-cell-mediated immune responses.[13,15−18] The core of GM3-presenting, lipid-coated NPs provides additional degrees of freedom for controlling the size, shape, and elasticity of the NPs, which are parameters that further influence the uptake and intracellular fate.[19−21]

Human immunodeficiency virus 1 (HIV-1) utilizes GM3-CD169-mediated binding to access nonendolysosomal compartments in macrophages and DCs, called virus-containing compartments (VCCs), which enhance HIV-1 transmission to T cells.[22−30] We have shown previously that GM3-presenting, lipid-coated gold and polymer NPs (GM3-NPs) bind to CD169-expressing macrophages and DCs[31−34] and that GM3-NPs colocalize with CD169$^+$ subcapsular macrophages in lymph nodes in vivo.[35] The intracellular fate of GM3-NPs in CD169$^+$ macrophages was found to be affected by the mechanical stiffness of the NP core, but gold or high-molecular-weight polylactic acid (PLA, molecular weight (Mw) = 209 000) NPs with sizes in the range between 80−150 nm successfully reconstituted HIV-1-like properties, including CD169-dependent capture and selective enrichment of NPs in VCC-like compartments in myeloid cells.[31−34] Intriguingly, GM3-presenting Au NPs were shown to accumulate at the interface between DCs and CD4$^+$ T cells.[36] However, it remains experimentally untested (i) whether GM3-NPs that bypass endocytosis remain accessible to T-cell surface functionalities when sequestered in VCCs of APCs, and (ii) if ligands associated with the NPs can activate T cells at the APC/T-cell interface. In this work, we investigate GM3-NPs with a biodegradable PLA polymer core as a platform for the APC-mediated activation of CAR T cells, utilizing Raji B cells and monocyte-derived DCs as APC models. The experimental strategy to control CAR T-cell activation at the IS developed in this work complements previous studies into the development of microparticle- or nanoparticle-based systems that mimic APCs (the so-called artificial APC, aAPC[37−39]) by displaying T cell activating and stimulating functionalities. Micrometer-sized aAPCs facilitate T cell activation and expansion ex vivo,[40] and nanoscale aAPCs used in vivo have shown promising therapeutic effects in animal models.[41−45] Generally, aAPCs allow strategies for the targeting and activation of T cells. Unlike aAPCs, GM3-NPs

https://doi.org/10.1021/acsnano.2c06516
ACS Nano XXXX, XXX, XXX−XXX

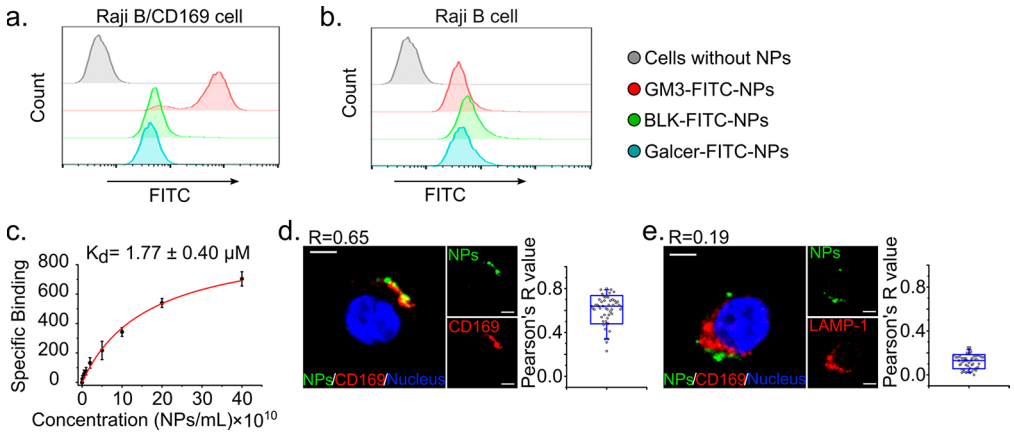

Figure 2. GM3-CD169-mediated targeting of GM3-FITC-NPs to Raji B/CD169 cell. (a, b) Representative flow cytometry histograms (FITC fluorescence) after incubation of specified NPs with Raji B/CD169 cells for 10 min at 37 °C. Conditions include cells without NPs treatment, and cells treated with GM3-FITC-NPs, BLK-FITC-NPs, and Galcer-FITC-NPs. (c) Binding curve for GM3-FITC-NPs binding with Raji B/CD169 cells. Fitted with one-site binding model. Specific binding was obtained by total binding from Raji B/CD169 cells subtracted by nonspecific binding from Raji B cells (n = 2). Data presented as average ± standard deviation. (d, e) Confocal sections of GM3-FITC-NPs associated with Raji B/CD169 cells. The cells were incubated with the NPs for 10 min and subsequently maintained at 37 °C for 4 h. The cells were stained for CD169 (panel (d)) and LAMP-1 (panel (e)). Pearson correlation coefficients (R) for NP signal and CD169 or LAMP-1 signal of 50 randomly selected cells are included in the box plots. Scale bar = 5 μm.

are designed not to mimic APCs but to recruit APCs for optimal activation of CAR T cells. We demonstrate that the GM3-NPs show a preferential localization at the interface between APC and CAR T cells where they colocalize with CARs. Increased CD69 expression and IL-2 secretion levels as well as F-actin and ZAP-70 enrichment at the IS confirm that NP-bound CAR ligands remain accessible to CAR T cells and achieve a strong APC-mediated CAR T cell activation.

RESULTS AND DISCUSSION

Synthesis and Characterization of FITC-Functionalized GM3-NPs for αFITC CAR T-Cell Activation. Here, we employed the CAR T cell, recognizing the small molecule FITC (αFITC CAR T cell) to probe and quantify CAR T-cell activation via FITC-functionalized GM3-NPs (Figure 1). The αFITC CAR contains the αFITC single-chain variable fragment (scFv) and CD8α hinge region in the extracellular domain, and CD28, 4−1BB, CD3ζ segments as well as a mCherry tag in the intracellular signaling domain (Figure 1a). The transduction efficiency, as assessed by the percentage of mCherry positive Jurkat T cells (cells with mCherry intensity higher than wild-type (WT) T cells), was >99% for the αFITC CAR T cells (Figure 1b). Confocal imaging of αFITC CAR T cells revealed that CARs were distributed over the entire cell surface (Figure 1c). GM3-functionalized NPs (GM3-NPs), consisting of a biodegradable high-molecular-weight polylactic acid (PLA) core coated by a lipid layer, were fabricated through one-step nanoprecipitation as described previously with detailed characterization.[33] The lipid layer was assembled from 55 to 57 mol % DPPC, 40 mol % cholesterol, 3 mol % GM3 as targeting functionality, and 0−2 mol % 1,2-dioleoyl-*sn*-glycero-3-phosphoethanolamine-*N*-(carboxyfluorescein) (18:1 PE CF, FITC-modified lipid) as CAR ligand (Figure 1d). The FITC-functionalized GM3-NPs (GM3-FITC-NPs) had an average hydrodynamic diameter of 126 ± 12 nm and a ζ-potential of −23 ± 4 mV. Scanning electron microscopy (SEM) images of GM3-NPs (Figure S1 in the Supporting Information) indicate a spherical morphology of the NPs. Other control NPs used in this work include FITC-functionalized NPs without GM3 (BLK-FITC-NPs) and FITC-presenting NPs with 3 mol % α-galactosylceramide (GalCer-FITC-NPs). The hydrodynamic diameters and zeta potentials for these NPs are included in Figure 1e. Galcer was included as negative control in this study, because the lipid has a similar glycolipid structure as GM3 but lacks the terminal sialic acid recognized by CD169. The lipid-coated polymer NPs exhibit excellent stability in cell culture medium at 37 °C over a period of 14 days (Figure 1f). A 22 nm increase in size when NPs were dispersed in cell culture medium (159 nm), compared to water (137 nm), may indicate some corona formation or a modest level of self-association of the NPs.

GM3−CD169-Mediated Binding of NPs to Raji B/CD169 Cells. Raji B cells stably transduced with CD169 (Raji B/CD169 cells[23]) were used as an APC model to evaluate APC-mediated activation of CAR T cells by GM3-FITC-NPs. Figures 2a and 2b shows fluorescence histograms obtained after incubating Raji B/CD169 and Raji B cells with GM3-FITC-NPs and control NPs. GM3-FITC-NPs binding to Raji B/CD169 cells was significantly higher than the nonspecific background binding observed for BLK-FITC-NPs or Galcer-FITC-NPs. In contrast, no specific binding of GM3-FITC-NPs was observed with Raji B cells. Fitting a one-site binding model to the GM3-FITC-NP binding curve as a function of NP input (and, thus, GM3 concentration, in units of μM) yields a dissociation constant of K_d = 1.77 ± 0.44 μM (Figure 2c, detailed calculation in the Supporting Information (SI)). The observed K_d value is significantly lower than the K_d value of individual GM3 molecules, confirming that the presentation of GM3 on the NP surface achieves a multivalent enhancement of the binding. Confocal maps of GM3-FITC-NPs 4 h after incubation with Raji B/CD169 cells are shown in Figures 2d and 2e. The NPs remain localized at or close to the cell surface in regions that are enriched in CD169 and that do not overlap with the lysosome marker LAMP-1, with Pearson correlation coefficients of R = 0.65 and 0.19, respectively. These observations imply that GM3-CD169-mediated binding of GM3-NPs to Raji B/CD169 cells avoids triggering an endolysosomal uptake, as is the case for CD169$^+$ DCs and

https://doi.org/10.1021/acsnano.2c06516
ACS Nano XXXX, XXX, XXX−XXX

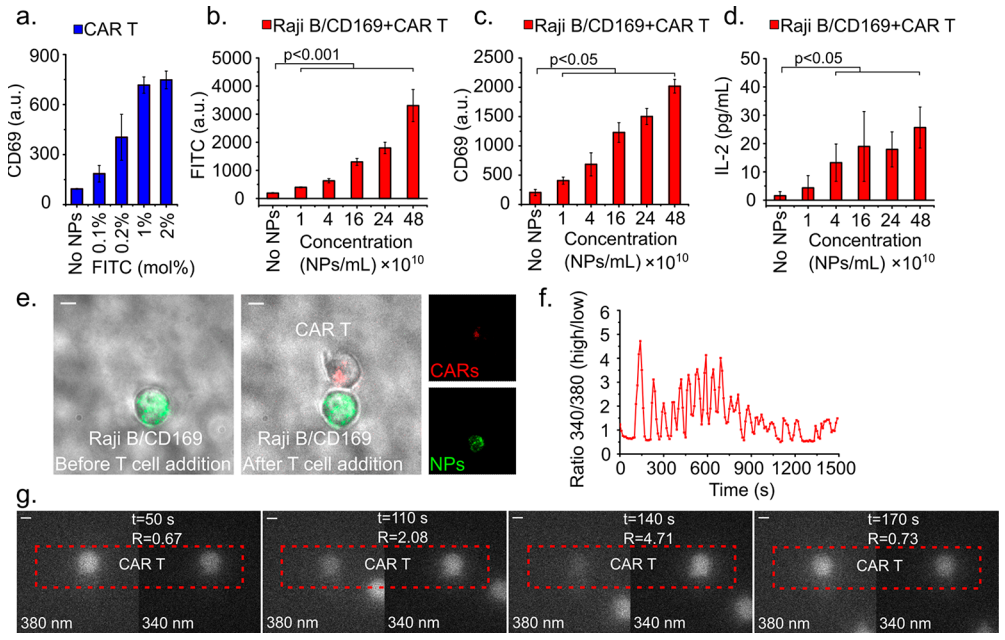

Figure 3. αFITC CAR T-cell activation by GM3-FITC-NPs associated with Raji B/CD169 (APC-mediated activation). (a) CD69 expression by αFITC CAR T cells after direct activation through GM3-FITC-NPs with different FITC concentrations incorporated in the membrane. (n = 2). (b–d) Characterization of αFITC CAR T cell activation through GM3-FITC-NPs associated with Raji B/CD169 cell (APC-mediated activation) by different markers: (b) Total FITC intensity of αFITC CAR T cell and Raji B/CD169 cell, (c) CD69 upregulation in αFITC CAR T cells, and (d) IL-2 secretion for specified input volumes of GM3-FITC-NPs (2 mol % FITC) (n = 4). (e–g) Ca^{2+} response of αFITC CAR T cell through GM3-FITC-NPs associated with Raji B/CD169 (APC-mediated activation): (e) bright-field view of GM3-FITC-NPs presenting Raji B/CD169 cell before and after CAR-T cell addition; (f) cellular Ca^{2+} activity in a CAR-T cell during the interaction with GM3-FITC-NPs presenting Raji B/CD169 cell monitored using the ratiometric Fura-2 AM dye (the ratio of the fluorescent intensities at 340 and 380 nm is plotted as a function of time); (g) representative time-lapse fluorescent images show Ca^{2+}activity of the CAR T cell. (scale bar = 5 μm). Data presented as average ± standard deviation. $p < 0.05$, $p < 0.01$, $p < 0.001$ by Student's t-test.

macrophages that collect GM3-NPs in nonendolysosomal VCCs.[31−34]

αFITC CAR T-Cell Activation by GM3-FITC-NP-Loaded Raji B/CD169 Cells. First, the direct activation of αFITC CAR T cells through free GM3-FITC-NPs was evaluated. To that end, GM3-FITC-NPs with different surface loadings of FITC were directly mixed with αFITC CAR T cells at a constant NP:cell ratio for 24 h before T cell activation was assessed. CD69 early activation marker was used to quantify the activation of αFITC CAR T cells through flow cytometry. These experiments revealed that CD69 expression in αFITC CAR T cells (Figure 3a) is correlated with the amount of FITC (mol %) incorporated in the lipid layer of the NPs. CD69 expression shows a clear increase as FITC concentration in the NP lipid layer is increased from 0.1 mol % to 2 mol %. As the CD69 expression level reached a plateau at a FITC input concentration of 2 mol %, we chose 2 mol % FITC for GM3-FITC-NPs synthesis for all subsequent experiments.

To characterize CAR T-cell activation through GM3-FITC-NPs associated with Raji B/CD169 (APC-mediated activation), Raji B/CD169 cells were first incubated with GM3-FITC-NPs for 10 min. After the removal of unbound NPs in three washing steps, αFITC CAR T cells were added at a ratio of 1:2 (Raji B/CD169:CAR T) and incubated for 24 h. For all input concentrations of GM3-FITC-NPs, the FITC intensity of cells, CD69 expression levels of CAR T cells, and the secretion of IL-2 as the second activation marker were significantly higher (except for IL-2 at the lowest input concentration) than for the mixture of Raji B/CD169 cells and CAR T cells without GM3-FITC-NPs (Figures 3b–d), indicating that Raji B/CD169 contact with T cells alone is insufficient to achieve a significant CAR T cell activation but that GM3-FITC-NPs associated with Raji B/CD169 provide a robust activation. Control experiments verified that free GM3-FITC-NPs, as well as GM3-FITC-NPs associated with Raji B/CD169 cells, do not activate WT T cells that lack CARs (see Figures S2a and S2b in the Supporting Informtion) and that GM3-NPs that lacked FITC ligand did not activate CAR T cells in cell-mediated exposure (Figure S2c in the Supporting Informtion). GM3-FITC-NPs binding to Raji B/CD169 cells results in an accumulation of GM3-FITC-NPs at or close to the plasma membrane of the APCs, and Figure 3b–d confirms that GM3-FITC-NPs remain accessible for CAR T cell activation when associated with Raji B/CD169 cells. A plot of the CD69 expression as a function of FITC intensity, which provides a measure for the number of GM3-FITC-NPs associated with the Raji B/CD169 cells in one case and for the number of free GM3-FITC-NPs directly bound to αFITC CAR T cells in the other, reveals that FITC achieves a stronger CAR T-cell activation if the activation is APC-mediated (Figure S2d in the Supporting Information). IL-2 secretion obtained under comparable FITC ligand concentrations was also higher for CAR activation through Raji B/CD169-associated GM3-NPs than for free GM3-NPs (Figure S2e in the Supporting Information), but this increase was not statistically significant.

Ca^{2+} influx represents a further key event downstream of T-cell receptor activation.[46,47] We monitored Ca^{2+} activity in αFITC CAR T cells preloaded with the Ca^{2+}-sensitive fluorescent dye, Fura-2AM, during their interaction with

https://doi.org/10.1021/acsnano.2c06516
ACS Nano XXXX, XXX, XXX−XXX

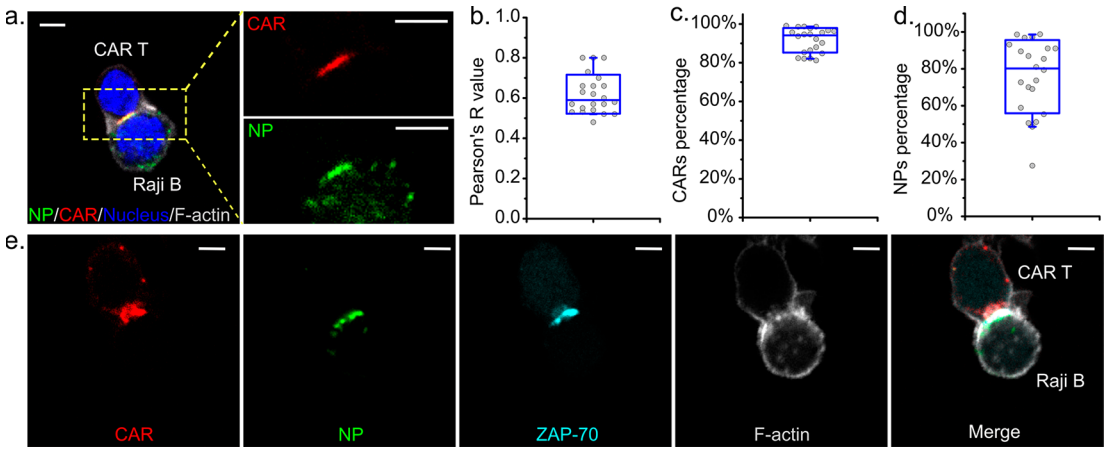

Figure 4. GM3-FITC-NP-induced synapse formation between αFITC CAR-T cell and Raji B/CD169 cell. (a) Confocal section of cell conjugate formed by αFITC CAR T cell and Raji B/CD169 cell. GM3-FITC-NPs (green), CAR (red), nucleus (blue) and F-actin (gray) were labeled. (b) Box plot of Pearson correlation coefficients (R) for CARs and NPs in individual cells. The average R is 0.62 ± 0.10. (c, d) Box plots of CAR localization at the cell−cell interface (panel (c)) and GM3-FITC-NPs localization at the cell−cell interface (panel (d)). The average CAR and NP localization at the IS is 92% ± 6% and 76% ± 20%, respectively (n = 22 for panels (b)−(d)). (e) Confocal section of αFITC CAR T cell−Raji B/CD169 cell conjugate with CAR (red), GM3-NP (green), ZAP-70 (cyan), and F-actin (gray) labeling. Scale bar = 5 μm.

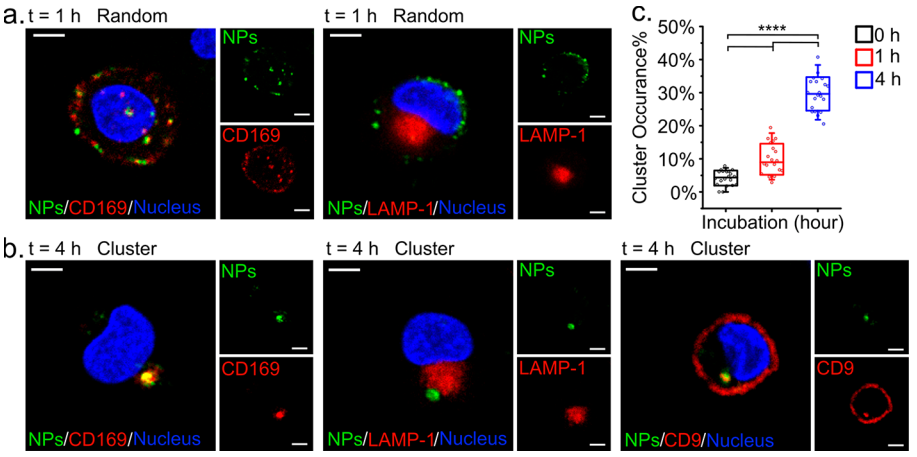

Figure 5. Intracellular fate of GM3-NPs in mature DCs. (a, b) Confocal maps of two phenotypes of GM3-FITC-PLA NPs in DCs after 15 min of incubation with NPs, and a subsequent chase of 1 and 4 h and staining for CD169 and LAMP-1. (a) Random distribution from 1 h incubation (b) Cluster distribution from 4 h incubation. (c) Dot plot of cluster phenotype occurrence over total cell number after 0, 1, and 4 h of incubation. Twenty confocal images with a total 1008 cells (0 h), 860 cells (1 h) and 955 cells (4 h) were collected and analyzed. Each dot represents the occurrence of cluster phenotype of total cells in one confocal image. Scale bar = 5 μm. Data presented as average ± standard deviation. [(****) p < 0.0001, per Student's t-test.]

GM3-FITC-NP-presenting Raji B/CD169 cells by measuring the fluorescence intensities at 510 nm when excited at 340 or 380 nm (a scheme of the experimental setup is provided in Figure S3 in the Supporting Information). When intracellular free Ca^{2+} binds to Fura-2, the peak excitation wavelength changes from 380 nm to 340 nm, whereas the peak emission at ~510 nm remains unchanged. Therefore, the ratios of the fluorescent intensities at 510 nm obtained when excited at 340 and 380 nm is directly related to the intracellular Ca^{2+} concentration. The bright-field images in Figure 3e show an immobilized Raji B/CD169 cell before and after the addition of a CAR T cell preloaded with Fura-2AM. After the binding of the CAR T cell to the GM3-FITC-NP-loaded Raji B/CD169 cell, the fluorescence intensity ratios reveal prolonged high-frequency Ca^{2+} oscillations in the CAR T cell for a duration of ~900 s (Figure 3f). Representative fluorescence images of the interacting αFITC CAR T and Raji B/CD169 cells at early time points (50, 110, 140, 170 s) illustrate the fluctuations in the intracellular Ca^{2+} concentration (Figure 3g). Unbound WT Jurkat T cells or WT Jurkat T cells in contact with GM3-FITC-NP-loaded Raji B/CD169 showed only basal levels of Ca^{2+} activity (Figure S4 in the Supporting Information).

Characterization of the Interface between Raji B/CD169 and αFITC CAR T Cells: GM3-NPs Accumulate at the IS, Induce CAR Polarization, and Recruit ZAP-70. Having demonstrated that GM3-FITC-NPs associated with Raji B/CD169 cells activate αFITC CAR T cells, we next sought to examine the IS formed between Raji B/CD169 cells and αFITC CAR T cells. To that end, Raji B/CD169 cells were first incubated with GM3-FITC-NPs. After removing unbound NPs by two washing steps, the cells were immobilized on a poly-L-lysine treated dish and incubated with αFITC CAR T cells for 1 h. Phalloidin staining revealed that F-actin is enriched at the contact interface between Raji

https://doi.org/10.1021/acsnano.2c06516
ACS Nano XXXX, XXX, XXX−XXX

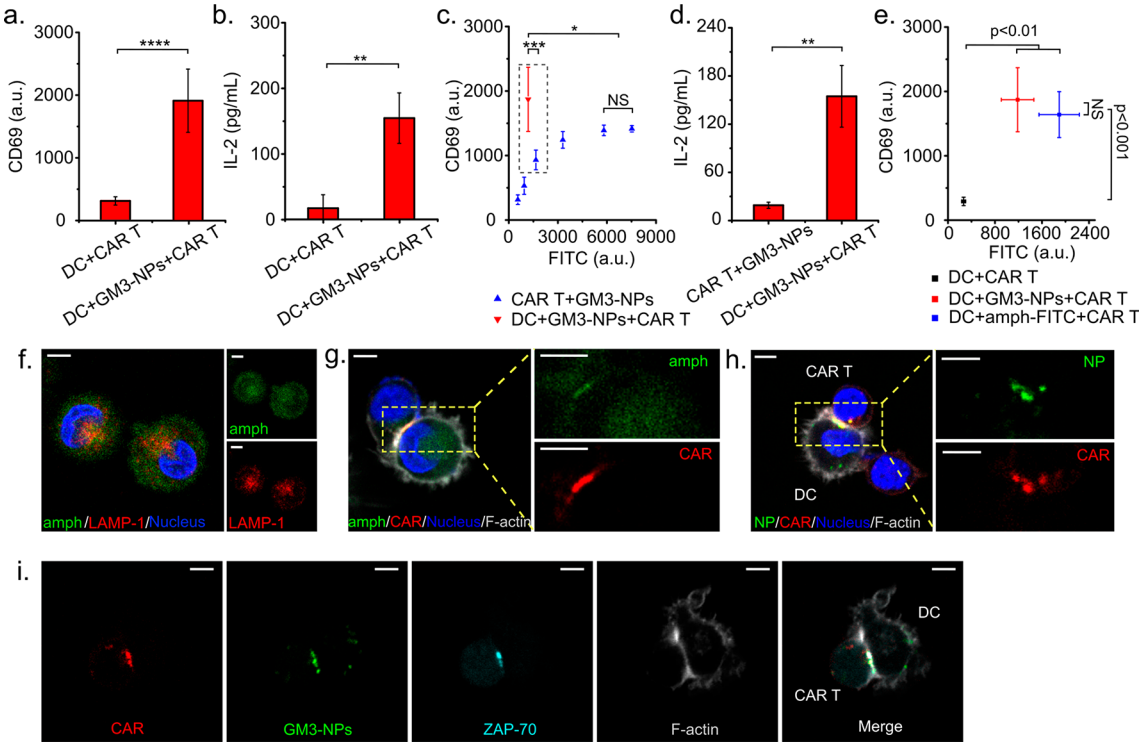

Figure 6. DC-mediated CAR T cell activation and synapse formation between GM3-FITC-NP-loaded DCs and CAR T cells. (a) CD69 expression and (b) IL-2 secretion for αFITC CAR T cells after incubation with DCs loaded with GM3-FITC-NPs or without (n = 4). (c) CD69 expression in CAR T cells, as a function of FITC signal intensity for direct activation by free GM3-NPs at different input concentrations (blue, n = 3) and APC-mediated activation (red, n = 4). (d) IL-2 secretion by CAR T cells for direct activation by free GM3-NPs versus for APC-mediated activation for the conditions marked by a dashed rectangle in panel (c). (e) CD69 expression in CAR T cells as a function of the FITC signal intensity for GM3-FITC-NPs, amph-FITC, and DC and CAR T cell mixture (without any FITC) as control. (n = 4). (f) Intracellular distribution of amph-FITC in DC after 1 h incubation. Lysosome were stained and labeled in red. (g) Cell conjugate formed by αFITC CAR T cell and DC after treatment with amph-FITC (green). (h) Cell conjugate formed by αFITC CAR T cell and GM3-FITC-NP-loaded DC. GM3-NPs (green), CARs (red), nucleus (blue), and F-actin (gray) were labeled. (i) Conjugate of αFITC CAR T cell and GM3-FITC-NP-loaded DC with CAR (red), GM3-NP (green), ZAP-70 (cyan), and F-actin (gray) labeling. Scale bar = 5 μm. Data presented as average ± standard deviation. [(*) p < 0.05, (**) p < 0.01, (***) p < 0.001, (****) p < 0.0001 by Student's t-test.]

B/CD169 and CAR T cells (Figure 4a). At this interface, which defines the GM3-NP-containing IS, both CARs and GM3-FITC-NPs are enriched and optically colocalize with Pearson correlation coefficients of R = 0.62 ± 0.10 (Figure 4b). In the confocal plane containing the cell−cell contact, 92% ± 6% of total CAR (Figure 4c) and 76% ± 20% of total GM3-FITC-NP (Figure 4d) fluorescence intensity was detected localized at the GM3-NP-containing IS. Zeta-chain-associated protein kinase 70 (ZAP-70), an important protein-tyrosine kinase for CAR T cell signaling upon antigen binding,[48,49] is also strongly recruited to the IS, where it shows a high level of optical colocalization with GM3-FITC-NPs and CARs (Figure 4e), confirming CAR T-cell activation through GM3-FITC-NPs at the immunological synapse.

Binding of GM3-NPs to Primary Mature DCs and Subsequent Intracellular Fate. So far, the investigations in this work have focused on Raji B/CD169 cells as an APC model. Next, we determined whether primary human CD169$^+$ DCs mediate a similar activation of CAR T cells and signal transfer at the GM3-NP-containing IS, as was observed for Raji B/CD169 cells. This validation is important as DCs are the most relevant APCs for T-cell priming in vivo.[50−52] Primary-monocyte-derived DCs were differentiated from CD14$^+$ peripheral blood monocytes and matured as described previously.[23] We first studied the binding and intracellular fate of GM3-NPs with DCs. Incubation of GM3-FITC-NPs with mature DCs led to two distinct phenotypes with different spatial GM3-NP distributions (see Figures 5a and 5b). In the "random" phenotype, the GM3-NP signal is distributed across the entire cell periphery, whereas the "cluster" phenotype contains the majority of NPs segregated in one compartment. CD169/LAMP-1 fluorescence immunostaining maps show that, for both phenotypes, GM3-FITC-NPs colocalize with CD169 but not with LAMP-1 (see Figures 5a and 5b). Importantly, the GM3-FITC-NP signal in the segregated clustered phenotype also colocalizes with the tetraspanin CD9 (Figure 5b), providing a staining pattern that is characteristic of VCCs.[26] The occurrence of the segregated cluster distribution significantly increases as a function of incubation time (t) as the comparison of the cluster probability for t = 0, 1, and 4 h in Figure 5c shows, suggesting that GM3-NPs were actively sequestered in specialized compartments within the cells, similar to what was observed previously for captured HIV-1 virus particles in mature DCs.[23,25,28,30] The formation of large GM3-NP clusters that are spatially separated from the plasma membrane is distinct for DCs and was not observed for Raji B/CD169 cells where NPs localized primarily at or close to the cell surface.

DC-Mediated CAR T Cell Activation and Characterization of the IS Formed between Primary DCs and CAR T Cells. To study the DC-mediated activation of CAR T cells, DCs were first incubated with GM3-FITC-NPs for 20 min.

https://doi.org/10.1021/acsnano.2c06516
ACS Nano XXXX, XXX, XXX−XXX

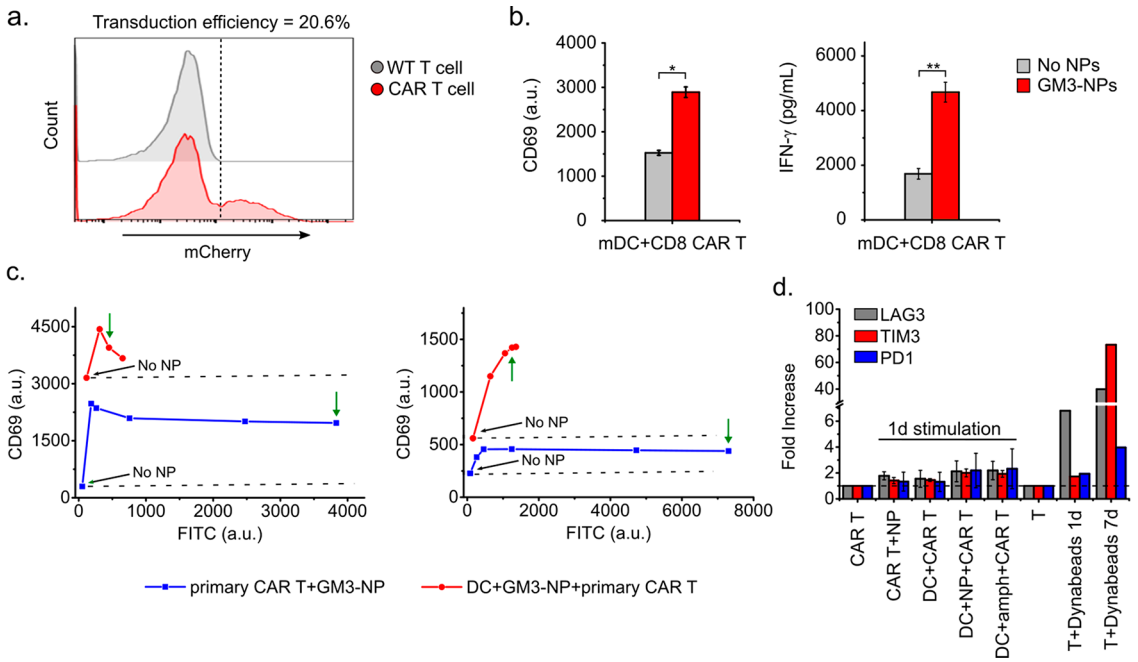

Figure 7. DC-mediated activation of primary CAR T cells. (a) Representative flow cytometry histogram (mCherry fluorescence) of transfected αFITC CD8⁺ CAR T cell (red) and wild-type T cell (gray). (b) CD69 upregulation and increased IFN-γ secretion αFITC CD8⁺ CAR T cell by GM3-FITC-NP-loaded DCs ($n = 2$). Data presented as average ± standard deviation. [(*) $p < 0.05$, (**) $p < 0.01$ by Student's *t*-test]. (c) CD69 expression in CD3⁺ CAR T cells, as a function of FITC signal intensity for direct activation by free GM3-NPs at different input concentrations (blue) and APC-mediated activation (red). Each plot represents results from the same DC and primary T-cell donor. (d) Fold increase of inhibitory receptors in CD3⁺ CAR T cells after 24 h of stimulation. Data represents average ± standard deviation from two independent experiments with DCs and primary T cells from two donors. The input concentrations of GM3-FITC-NPs used for the exhaustion experiments are marked with green arrows in panel (c).

After the removal of unbound NPs in three washing steps, αFITC CAR T cells were added at a ratio of 1:2 (DC:CAR T) and incubated for 24 h. Figures 6a and 6b shows CD69 expression and IL-2 secretion as markers for CAR T-cells activation obtained with DCs in the presence or absence of GM3-FITC-NPs. CD69 expression and IL-2 secretion are significantly increased for CAR T cells treated with GM3-FITC-NP-loaded DCs (APC-mediated activation) when compared to preparations in which CAR T cells were mixed with DCs without GM3-FITC-NPs. The data confirm that GM3-FITC-NPs associated with the APCs achieve a pronounced increase in the activation of CAR T cells. Figure 6c compares the APC-mediated activation of CAR T cells by GM3-FITC-NPs with the direct activation through different concentrations of free GM3-FITC-NPs. The plot shows CD69 expression, as a function of FITC intensity, which provides a measure for the number of GM3-FITC-NPs associated with DCs in one case and for the number of GM3-FITC-NPs directly bound to CAR T cells in the other. Importantly, APC-mediated activation achieves significantly higher CD69 expression levels than the direct activation, even when the FITC intensities are substantially higher for the latter. Figure 6d shows IL-2 secretion levels for conditions with nearly identical FITC intensities marked in the gray box in Figure 6c. Consistent with the findings for CD69, IL-2 secretion levels are significantly higher for the APC-mediated activation than for the direct activation of CAR T cells.

It can be instructive to compare the CAR T-cell activation obtained with GM3-FITC-NP or amph-FITC (18:1 PE CF, FITC modified lipid) treated DCs at the same FITC input concentration. Figure 6e shows CAR T-cell CD69 expression levels, as a function of FITC signal intensity for GM3-FITC-NPs, amph-FITC, and DC and CAR T cell mixture (without any FITC) as control. Amph-FITC ligands yield an overall significantly higher FITC intensity than GM3-FITC-NPs, presumably due to an efficient insertion into the cell membrane via the lipid tail. Despite a higher FITC concentration associated with the cells in the case of amph-FITC ligands, the CD69 expression level is comparable to that observed for GM3-FITC-NPs. Both are significantly higher than for the mixture of DCs and CAR T cells control. Confocal analysis of the amph-FITC distribution obtained after an incubation period of 1 h reveals that the ligand is distributed across the cell (Figure 6f) with a modest enrichment at the IS formed between CAR T cell and DC where the CARs are localized (Figure 6g). In contrast, GM3-FITC-NPs show a strong preferential localization at the DC − CAR T cell interface where they optically colocalize with CARs (Figure 6h).

The spatial pattern observed with GM3-FITC-NPs in DC−CAR T cell contact areas closely resembles that observed for Raji B/CD169−CAR T cell pairs. Immunostaining also confirms the recruitment of ZAP-70 to the IS (Figure 6i), and the high degree of optical colocalization between ZAP-70 and CAR is consistent with CAR T-cell activation by GM3-FITC-NPs. Although the GM3-FITC-NP sequestration in VCC-like structures in the absence of CAR T cells is found in DCs but not Raji B/CD169 cells, the enrichment of GM3-FITC-NPs, CARs, and F-actin at the cell contact, as well as the recruitment of ZAP-70, resembles the structural patterns observed at the IS formed between a CAR T cell and Raji B/CD169 cell as APC model.

https://doi.org/10.1021/acsnano.2c06516
ACS Nano XXXX, XXX, XXX−XXX

Additional experiments performed with a 2.5 h preincubation step of DCs and GM3-NPs prior to addition of CAR T cells also showed a preferential localization of the FITC signal at the cell interface between APCs and T cells (see Figure S5a in the Supporting Information). In the case of DC-mediated HIV-1 transmission to T cells, GM3-CD169 mediated localization within VCCs and redistribution to the infectious synapse upon T cell addition has been observed,[22,23,53] and it is indicated that intracellular VCCs formed in the absence of T cells are redistributed and transported to the infectious synapses after T cell addition.[26,54] The strong polarization of GM3-FITC-NPs to the IS observed in this work suggests that GM3-NPs trigger similar cellular mechanisms as HIV-1 to achieve an enrichment at the IS between APC and CAR T cell.

To test how the stimulatory effect of DC-associated GM3-FITC-NPs in CAR T cells decreased as a function of time, DCs were maintained after exposure to GM3-FITC-NPs for 0−20 h before T cells were added (see Figure S5b in the Supporting Information). After the preincubation period of 20 h, the NP-containing DCs still induce CD69 expression in CAR T cells (35.5% of the CD69 expression achieved, relative to that observed without any preincubation). Importantly, CD69 expression on CAR T cells induced by DC-associated GM3-FITC-NPs remained above the level achieved with DC and CAR T cell cocultures in the absence of GM3-NPs throughout the duration of the experiment, confirming that a significant fraction of the FITC ligand on DCs remained accessible for CAR T-cell activation.

DC-Mediated Activation of Primary CAR T Cells. All results discussed so far were obtained with Jurkat CAR T cells. To test the ability of the proposed antigen presenting platform to activate CARs in human primary T cells, primary $CD8^+$ T cells were engineered to express the αFITC CAR through lentiviral transduction. The transduction efficiency, as assessed by the percentage of mCherry positive cells, was 20.6% (Figure 7a). Exposure of the engineered αFITC $CD8^+$ CAR T cells to GM3-FITC-NP-loaded DCs resulted in T-cell activation. Figure 7b shows αFITC $CD8^+$ T cells activation quantified by CD69 upregulation and IFN-γ secretion after 24 h of incubation. In the case of GM3-FITC-NPs-treated DCs, CD69 was significantly upregulated with a 1.9-fold induction (fold induction is defined as the geometric mean fluorescence intensity (GeoMFI) of CD69 fluorescence intensity obtained with GM3-FITC-NPs divided by the GeoMFI of CD69 without the addition of NPs). The IFN-γ secretion was also significantly increased upon coculture with GM3-FITC-NP-loaded DCs. Overall, the data confirm that GM3-FITC-NPs facilitate the APC-mediated activation of primary $CD8^+$ CAR T cells.

Two independent activation experiments obtained with cells from two different donors were performed to compare the free GM3-FITC-NP- and APC-mediated activation. Figure 7c shows that primary CAR T cells are sensitive toward stimulation with free GM3-FITC-NPs and reaches saturated activation levels at low dosage. GM3-FITC-NPs associated with DCs achieved even higher CD69 expression in primary CAR T cells than free GM3-NPs. Exhaustion in CAR T cells can arise via persistent stimulation to the cells during ex vivo expansion.[55] To evaluate the exhaustion of primary CAR T cells, the expression levels of inhibitory receptors LAG-3, TIM-3, and PD-1 were quantified after 24 h of stimulation (Figure 7d). Fold increase of the inhibitory receptors relative to CAR T cells without stimulation was used to quantify expression. Free GM3-FITC-NP-mediated CAR T-cell activation resulted in a 1.8-fold, 1.4-fold, and 1.3-fold increase of LAG-3, TIM-3 and PD-1, respectively. Cocultures of primary CAR T cells and DCs, in the absence of GM3-FITC-NPs, yielded essentially identical inhibitor receptor expression levels, as observed for free GM3-FITC-NP-mediated activation. Activation of CAR T cells through GM3-FITC-NP-treated DCs led to a 2.1-fold increase of LAG-3, 2.0-fold increase of TIM-3, and 2.2-fold increase of PD-1. Interestingly, GM3-FITC-NP- and amph-ligand-treated APCs induced comparable exhaustion levels for identical FITC input concentrations. As an additional benchmark, we also included primary T cells (without CAR) stimulated by CD3/CD28 Dynabeads for 1 and 7 days. After 1 day of stimulation, primary T cells exhibited a 6.8-fold increase of LAG-3 and this value exceeded those observed for GM3-FITC-NPs and CAR T cells under comparable conditions. In the case of TIM-3 and PD-1, the GM3-FITC-NP treated APC-mediated activation to primary CAR T cells resulted in a higher increase in expression (2.0-fold and 2.2-fold) than for the Dynabead-induced stimulation of T cells (1.7-fold and 1.9-fold). After 7 days of stimulation through Dynabeads, the inhibitory receptor expression level of T cells further significantly increased (41, 74, 4.1-fold increases were observed for LAG-3, TIM-3, and PD-1, respectively).

CONCLUSION

Priming of CAR T cells through APCs in lymph nodes is considered a potential strategy to enhance their persistence and activity.[2] This approach requires adequate carriers that can transport CAR ligands to APCs in lymph nodes. We have investigated ganglioside-functionalized lipid-coated NPs with a biodegradable, high-molecular-weight polylactic acid core as carriers for CAR ligands that enrich at the IS. The GM3-NPs bind specifically to CD169 expressing Raji B cells and DCs and avoid endocytosis. Instead, the GM3-NPs remain in non-endolysosomal compartments at the membrane of Raji B/CD169 cells or are sequestered into VCC-like compartments in DCs. CAR T cells are activated both through GM3-FITC-NP-loaded Raji B/CD169 cells and DCs, as well as through free GM3-FITC-NPs. However, APC-mediated activation results in higher CD69 expression than free GM3-FITC-NP-mediated activation at a comparable FITC concentration (see Figures 6c and 6d, as well as Figure S2d in the Supporting Information and Figure 7c). Several effects may account for this outcome:

(1) Ligand-mediated receptor dimerization is critical for CAR T cell activation, which benefits from spatial CAR clustering.[49] Free GM3-FITC-NPs only provide nanoscale CAR clustering within the footprint of the NP, whereas GM3-FITC-NPs collected and locally concentrated by APCs can provide CAR clustering for much longer (micrometer) length scales (see Figures 6h and 6i, and Figure 4).

(2) Antigen recognition and T-cell receptor (TCR) signaling have a mechanical component that is dependent on force generation by the actin cytoskeleton,[56,57] and efficient force-dependent signaling may require the formation of an IS-like cell contact between CAR T cell and APC.[58]

(3) CD80 and CD86 expression levels are significantly upregulated in mature DCs,[59] and these costimulatory signals provided at the IS are expected to strengthen the activation of the CAR triggered through recognition of its ligand.[3] Future studies will quantify the relative contributions from these effects. This work examined the cellular interface between APC

https://doi.org/10.1021/acsnano.2c06516
ACS Nano XXXX, XXX, XXX−XXX

and CAR T cell where the CAR signal is transduced for both Raji B/CD169 and DCs. In both cases, GM3-NPs and CARs accumulate and optically colocalize at the cell contact interface, with enrichment of F-actin and recruitment of ZAP-70, which is indicative of the formation of a GM3-NP-containing functional IS. Importantly, it was demonstrated that CAR ligands bound to GM3-NPs remain accessible to the CAR T cell in the IS.

Although this work utilized FITC-specific CAR T cells as models to address the fundamental question whether GM3-PLA-NPs achieve CAR T-cell activation at the immunological synapse, the FITC-specific CAR T cells also have some relevance for cancer therapy, because they play a role in emerging universal CAR T-cell strategies.[60−62] For instance, by linking FITC to functionalities that recognize tumor-specific antigens,[63] it becomes feasible to deploy αFITC CAR T cells against a range of antigens, providing a potential strategy to reduce the costs associated with CAR fabrication.[64] Therefore, αFITC CAR T cells and strategies to efficiently stimulate them are of high general interest. Importantly, amph-FITC ligands have previously been shown to efficiently activate CAR T cells when presented on DCs. However, amph ligands lack binding specificity for DCs and show quick internalization. These effects may result in undesired side effects and fast decay in vivo. Interestingly, under the in vitro conditions of this work, GM3-FITC-NPs achieved a much more preferential localization at the IS than amph-FITC ligands, which could be advantageous for CAR T-cell activation. This preferential localization of GM3-NPs to the IS resulted in an APC-mediated CAR T-cell activation, as measured by CD69 expression, that was at least as good as that for amph-ligands, even though the overall cell associated FITC concentration was lower. Amph-ligands have already demonstrated their efficacy in vivo, whereas, for GM3-NPs, this key test is still missing, and it cannot be excluded that GM3-NPs are less effective in vivo. Preliminary mouse studies indicate that GM3-PLA-NPs reach secondary lymphoid tissues (spleen and LNs) after intravenous injection (see Figure S6 in the Supporting Information). The prospect of targeting secondary lymphoid tissues together with the key finding of this work that GM3-NPs provide opportunities for engineering selective and prolonged ligand presentation at the cellular nexus relevant for persistent, cell-mediated T cell activation warrants future studies to validate the potential of GM3-NPs to stimulate lymphocytes in vivo.

METHODS

Cell Culture. Raji B cells were cultured in complete RPMI-1640 medium (Gibco, Thermo Fisher Scientific, No. 11875093) containing 10% FBS (Gibco, Thermo Fisher Scientific, No. 16000044) and 1% penicillin−streptomycin (Gibco, Thermo Fisher Scientific, No. 15070063). Raji B cells were transduced with VSV-G pseudotyped LNC-CD169 mutant retroviral vectors, followed by 1 mg/mL G418 (Gibco, Thermo Fisher Scientific) selection, as described previously.[23] $CD14^+$ monocytes were differentiated into immature dendritic cells in complete RPMI-1640 medium supplement with IL-4 and GM-CSF for 5 days. Dendritic cells were matured by adding 100 ng/mL LPS for 24 h. HEK293FT cells were cultures in Dulbecco's modified Eagle's medium (DMEM) supplemented with 10% FBS, penicillin/streptomycin (Corning), L-glutamine (Corning), and 1 mM sodium pyruvate (Lonza). Jurkat T cells and CAR T cells were cultured in RPMI-1640 medium containing 5% FBS and 1% penicillin−streptomycin. $CD8^+$ primary T cells and CAR T cells were cultured in human T cell medium consisting of X-Vivo 15 (Lonza No. 04−418Q), 5% Human AB serum (Valley Biomedical No. HP1022), 10 mM *N*-acetyl L-cysteine (Sigma−Aldrich, No. A9165), 55 μM 2-mercaptoethanol (Thermo Scientific, No. 31350010) supplemented with 100 units/mL IL-2 (NCI BRB Preclinical Repository). All cells were cultured at 37 °C in a humidified atmosphere containing 5% CO_2.

Lentivirus Generation and Transduction of Jurkat T Cells. Jurkat T cells were maintained in complete RPMI-1640 media as described above. For transduction, replication-incompetent lentivirus was packaged via PEI transfection of HEK293FT cells in a 6-well plate with lentiviral packaging and envelope plasmids (pDelta, Vsvg, and pAdv) and the anti-FITC CAR construct (3rd generation of CAR construct) in a pHR lentiviral expression vector. Virus-containing supernatant was collected 3 days post-transfection and spun down to remove cell debris. A quantity of 5×10^5 Jurkat cells were infected with between 500 μL and 1 mL of anti-FITC CAR viral supernatant then diluted with 4 mL of complete RPMI media 24 h post-infection. Four days after infection, transduced Jurkat cells were analyzed via flow cytometry to assess transduction efficiencies and anti-FITC CAR expression via mCherry tag.

Primary T-Cell Isolation and Transduction. Anonymized whole peripheral blood was obtained from Boston Children's Hospital and primary $CD8^+$ T cells were isolated using the STEMCELL $CD8^+$ Enrichment cocktail and RosetteSep system. $CD8^+$ T cells were cryopreserved in 90% human Ab serum (Valley Biomedical) and 10% DMSO. Two days prior to transduction, T cells were thawed and activated with ImmunoCult human CD3/CD28 T cell activator (STEMCELL).

For transduction, replication-incompetent lentivirus was packaged via PEI transfection of HEK293FT cells in a T175 flask with lentiviral packaging and envelope plasmids and the anti-FITC CAR construct. One day after transfection, the HEK293FT culture media was removed and replaced with prewarmed FreeStyle 293 expression medium (Gibco) supplemented with 100 U/mL penicillin, 100 μg/mL streptomycin, 1 mM sodium pyruvate, and 5 mM sodium butyrate. Beginning 48 h post-transfection, viral supernatant was collected and replenished with fresh FreeStyle 293 media for 3 days. Then, the harvested lentivirus was concentrated using a 40% (w/v) PEG-8000 and 1.2 M NaCl solution overnight and spun down for 1 h at 1600 g at 4 °C. One day prior to transduction, T cells were activated with Immunocult Human CD3/CD28 T cell Activator, according to manufacturer instructions. In addition, a non-TC-treated 6-well plate was coated with 20 μg/mL of Retronectin in PBS and left at 4 °C overnight. For primary T-cell transduction (either second or third generation of CAR construct), all of the concentrated virus collected from one T175 flask was spun onto one well of the Retronectin-coated plate for 90 min at 1200 g. The viral supernatant was then removed and 4 mL of activated primary $CD8^+$ T cells was added and incubated for 72 h at 37 °C before moving to a T75 flask for expansion. Primary CAR T cell used in Figures 7c and 7d are $CD3^+$ CAR T cell. Transduction efficiencies were analyzed via mCherry tag or V5 tag (Invitrogen, No. 25679642).

Preparation of Lipid-Coated Polymer NPs. All lipids were purchased from Avanti Polar Lipids. High-molecular-weight PLA (poly(D,L-lactide) ester terminated, R207S with intrinsic viscosity of 1.3−1.7 dL/g and molecular weight of 209 000[65] were purchased from Sigma−Aldrich. Lipid-coated polymer NPs were synthesized through a one-step nanoprecipitation method, as previously described.[33] The volume ratio of aqueous to organic solution was chosen to be 10:1, using a lipid/polymer weight ratio of 15%[66] (under this condition, the total lipid amount is 0.25 μmol). To prepare GM3-NPs, lipid mixture containing DPPC (25 mg/mL), cholesterol (25 mg/mL), GM3 (2 mM), and 18:1 PE CF (1.1 mM) with 55:40:3:2 molar ratio in chloroform were added to 4 mL of Milli-Q water. Next, 0.4 mL PLA solution in acetonitrile (2.5 mg/mL) was pipetted dropwise to the aqueous solution. The final solution was vortexed for 10 s and sonicated in a bath sonicator (Branson Ultrasonics, No. 5510). Next, NPs were washed 3 times (4500*g*, 15 min) using 10 kDa Amicon Ultra-4 centrifugal filter (Millipore Sigma) to remove organic solvent and free lipid molecules. The final volume of samples was

https://doi.org/10.1021/acsnano.2c06516
ACS Nano XXXX, XXX, XXX−XXX

adjusted to 100 μL. A typical 10^{11} NPs in 100 μL sample with 10^{12} NPs/mL can be obtained (detailed calculation is given in the Supporting Information). The PLA NP core has a glass-transition temperature of T_m = 41.9 ± 0.3 °C and Young's modulus of E = 1.41 ± 0.67 GPa.[33] To prepare BLK-NPs, molar ratio of 58% DPPC, 40% cholesterol and 2% 18:1 PE CF were used. To prepare Galcer-NPs, GM3 were replaced by using 3% D-galactosyl-β-1,1′ *N*-palmitoyl-D-erythro-sphingosine (2 mM). Amph-FITC ligand was prepared by dissolving 18:1 PE CF in PBS at 0.25 mM.

Characterization of GM3-NPs. Hydrodynamic size and zeta potential measurements were performed using Zetasizer Nano ZS90 (Malvern). For hydrodynamic size measurements, NPs were diluted with Milli-Q water. Colloidal stability of NPs was monitored in the cell culture media (10% FBS RPMI) at 37 °C. The zeta potential of NPs was measured in 10 mM NaCl solution. The absorption of GM3-FITC-NPs in Milli-Q water were acquired using Spectronic 200 UV−vis spectrometer (Fisher Scientific). Milli-Q water was used for baseline correction. Beer's law was used to calculate the concentration of NPs using the absorption value of FITC at wavelength of 485 nm, and molar absorptivity of ε = 75 000 M^{-1} cm^{-1}. SEM imaging was performed using a Zeiss Supra 55 system. To prepare SEM samples, a glass substrate was treated with poly-L-lysine for 15 min. Upon removal of poly-L-lysine, 10-fold diluted sample was then deposited dropwise onto the substrate and incubated for 20 min, removed, and air-dried.

Characterization of GM3-CD169 Binding in Raji B/CD169 Cells. Quantities of 5 ×10^5 Raji B/CD169 and Raji B cells were pelleted after centrifugation (270 g, 5 min). 2% 18:1 PE CF were incorporated to all NPs for labeling. GM3, GalCer and without any glycosphingolipids (blank) NPs (1.5 × 10^{10} in 0.1 mL of 10% FBS RPMI-1640) were added to the cell pellets and incubated at 37 °C for 10 min. A binding curve were obtained by using between 10^8 and 4 × 10^{10} GM3-NPs in 0.1 mL of 10% FBS RPMI-1640. Unbound NPs were washed by centrifugation (270 g, 5 min, 2 times), and cells were fixed with 4% paraformaldehyde (PFA) for 10 min at room temperature. Following the last washing step, the fluorescence intensity of each sample was measured by flow cytometry using a FACSCalibur instrument (BD Biosciences). Data were analyzed through FlowJo 10. All fluorescence intensities were background corrected (cells without treatment were used as background).

Intracellular Trafficking of GM3-FITC-NPs in Raji B/CD169 cells and DCs. 5 ×10^5 Raji B/CD169 cells were incubated with 2 × 10^{10} GM3-NPs in 0.1 mL media for 10 min at 37 °C. 4 ×10^5 DCs were incubated with 1.5 × 10^{10} GM3-NPs in 0.1 mL media for 15 min at 37 °C. Unbound NPs were removed by centrifugation (270 g, 5 min, 2 times). Following the washing step, cells were dispersed in 0.5 mL media and incubated for 4 h at 37 °C. Cells were subsequently stained with 1 μg/mL Hoechst 33342 for 15 min at 37 °C. Cells were then dispersed in 1 mL media and seeded in poly-L-lysine (Sigma No. P4707)-treated 35-mm glass bottom dishes (Cellvis) for 15 min at 37 °C. Unbound cells were removed and cells were gently washed with 1× PBS. Cells were then fixed in 4% PFA for 10 min, permeabilized with 0.1% Triton X-100 for 12 min and blocked with 1% BSA solution for 30 min at room temperature. To stain CD169, CD9 and LAMP-1, 1 μg/mL antihuman CD169 (Sialoadhesin, Siglec-1, Clone: 7-239), antihuman CD9 (Clone: HI9a) and antihuman CD107a (LAMP-1, Clone: H4A3) mAbs (BioLegend) were added and incubated overnight at 4 °C. One μg/mL Alexa Fluor 647 (Goat antimouse, Clone: Poly4053) conjugated secondary antibody (BioLegend) was subsequently added and incubated for 1 h at room temperature. Multiple washing steps (1× PBS) were performed after incubation with primary and secondary antibodies. Cells were dispersed in 1.5 mL of 1× PBS for confocal imaging with an Olympus Model FV3000 scanning confocal microscope.

αFITC CAR T-Cell Activation. 10^9 GM3-FITC-NPs with 0.1−2 mol % FITC input loadings were added to 4 × 10^5 αFITC CAR T cells in a 96-well plate and incubated for 24 h at 37 °C. For APC-mediated CAR T-cell activation, 2:1 T/APC cell ratio was used. 2 × 10^5 Raji B/CD169 cells were first incubated with between 1 × 10^9 and 4.8 × 10^{10} GM3-FITC-NPs in 0.1 mL media for 10 min at 37 °C. For mature DCs, 2 × 10^5 DCs were first incubated with 2.4 × 10^{10} GM3-FITC-NPs (corresponding to 1.2 nmol FITC lipid) or 1.2 nmol amph-FITC ligand (18:1 PE CF) in 0.1 mL media for 20 min at 37 °C. Unbound NPs or amph-ligands were removed by centrifugation (270 g, 5 min,3 times). Raji B/CD169 cells or DCs presenting GM3-FITC-NPs were then mixed with 4 × 10^5 αFITC CAR T cells in a 96-well plate and the cell mixture were incubated for 24 h at 37 °C. For the activation with a "pre-incubation", DCs after exposure to GM3-NPs (unbound GM3-NPs were removed and DCs were washed three times) were maintained at 37 °C for 0−20 h and washed once before mixing with CAR T cells. For direct CAR T-cell activation, between 2 × 10^8 and 2.4 × 10^{10} GM3-FITC-NPs were added to 4 × 10^5 αFITC T cells in a 96-well plate and incubated for 24 h at 37 °C. The volume of media in each well was adjusted to 300 μL. Early activation marker CD69 was used to quantify T-cell activation level. To stain CD69, cells were pelleted at 240 g for 5 min followed by two washing steps in FACS staining buffer (1% BSA, 0.1% NaN_3 and 2 mM EDTA in 1× PBS). 0.1 mL 2 μg/mL APC conjugated mouse antihuman CD69 (BD Biosciences #560711) were then added and incubated for 30 min at 4 °C. Cells were washed twice and dispersed in FACS staining buffer. Samples were measured by LSR II flow cytometer (BD Biosciences). For the exhaustion experiments, after the 24 h activation of primary CAR T cells, the cells were collected and stained for 30 min at room temperature with PE-Cy7 conjugated PD-1 antibody (Invitrogen, No. 25279941), APC conjugated LAG-3 antibody (Invitrogen, No. 17223941), and Super Bright 702 conjugated TIM-3 antibody (Invitrogen, No. 67310941). Samples and compensation beads (Invitrogen OneComp eBeads, No. 01111142) were measured by an Attune NxT flow cytometer. For the activated T-cell control samples, primary human T cells were thawed into complete XVIVO15 media and allowed to recover for 24 h. Dynabeads Human T-Activator CD3/CD28 beads (ThermoFisher, No. 11131D) were added at a bead:T cell ratio of 1:1, according to manufacturer instructions. Cells were maintained for 7 days then collected and stained with the same PD-1, LAG-3, and TIM-3 antibodies as previously described. Data were analyzed by Flowjo 10 software. Living cells were first gated followed by gating CAR T cells. GeoMFI of FITC signal and CD69 expression were obtained from living cells and CAR T cells, respectively. IL-2 and IFN-γ secretion in cell culture supernatant were quantified by ELISA, following the manufacturer's instructions (BD Biosciences, Nos. 555190 and 555142).

Ca^{2+} Signaling. 5 ×10^5 αFITC Jurkat CAR T cells were loaded with 1.5 μM fura-2 AM indicator in 1× PBS and incubated for 15 min at 37 °C. T cells were washed and dispersed in 1 mL media and incubated for an additional 30 min to allow complete de-esterification of intracellular AM esters. 2.5 × 10^5 Raji B/CD169 cells were incubated with 3 × 10^{10} NPs in 0.1 mL media for 10 min at 37 °C. Unbound NPs were removed by centrifugation (270 g, 5 min, 2 times). Raji B/CD169 cells were then dispersed in 0.5 mL media and seeded in poly-L-lysine treated 35 mm glass bottom dishes (Cellvis) for 15 min at 37 °C. Unbound cells were removed and cells were gently washed with 1× PBS. Cells were dispersed in 1.5 mL media and imaged with modified Olympus Model IX71 inverted microscope (Figure S3 in the Supporting Information). CAR T cells were subsequently added dropwise by a syringe to the dish. Bright-field scattering images were illuminated with a 100 W tungsten lamp through a bright-field condenser (NA = 0.55) and were collected with a 60× oil objective with adjustable numerical aperture (NA = 0.65−1.25). Monochromatic images were recorded with an Andor ixon electron multiplying charge-coupled-device detector (EMCCD) camera. Fluorescence imaging was performed under epi-illumination, using appropriate excitation and emission filters and dichroics. For Ca^{2+} signaling, 380 and 340 nm excitation filters were installed in a filter wheel and were controlled by a Lambda 10−3 controller. Speed 3 (50 ms for neighboring filter positions) for active filter wheel was selected. Exposure time at 380 and 340 nm was 100 and 300 ms, respectively. Images at 380 and 340 nm were taken every 10 s for defined period.

https://doi.org/10.1021/acsnano.2c06516
ACS Nano XXXX, XXX, XXX−XXX

Conjugation Formation. 2×10^5 Raji B/CD169 cells were incubated with 2×10^{10} GM3-FITC-NPs in 0.1 mL media for 10 min at 37 °C. 2×10^5 DCs were incubated with 2×10^{10} GM3-FITC-NPs or 1 nmol amph-FITC ligand (18:1 PE CF) in 0.1 mL media for 20 min at 37 °C. Cells were washed in PBS and unbound NPs were removed by centrifugation (270 g, 5 min, 2 times). Cells were subsequently dispersed in 0.5 mL media and transferred to poly-L-lysine pretreated 35-mm glass-bottom dishes (Cellvis). Unbound cells were removed by gentle wash. 4×10^5 αFITC Jurkat CAR T cells dispersed in 1.5 mL media were added to the dish and incubated for 1−1.5 h at 37 °C. Cells were stained with 2 μg/mL Hoechst 33342, fixed in 4% PFA, permeabilized in 0.1% Triton X-100, blocked in 1% BSA solution and stained with 3× Alexa Fluor 647 Phalloidin (Invitrogen). To stain ZAP-70, after the incubation, cells were fixed, permeabilized, blocked, and stained with 4 μg/mL Alexa Fluor 647 ZAP-70 monoclonal antibody (eBioscience, Clone: 1E7.2) at 4 °C overnight followed by F-actin staining with 3× Alexa Fluor Plus 405 Phalloidin (Invitrogen). Cell membrane was stained using 0.5 × CellMask Deep Red plasma membrane stain for 5 min at 37 °C. Cells were dispersed in 1.5 mL 1 × PBS for confocal imaging with an Olympus Model FV3000 scanning confocal microscope.

In Vivo GM3-NP Delivery. Female NU+ immunocompetent mice, 6−8 weeks of age, were purchased from Charles River Laboratories (No. 089, NU/NU heterozygous) and were used for in vivo GM3-NPs delivery experiments. Animal studies were conducted at the Boston University Medical School Animal Science Center, under a protocol approved by the Boston University Institutional Animal Care and Use Committee. All animal experiments were performed in accordance with the relevant institutional and national guidelines and regulations. To measure the in vivo distribution of GM3-NPs, the 18:1 PE CF in the lipid layer was substituted into 18:0 Cy5 PE (excitation/emission 640/680 nm). PEGylated lipids were added to the lipid layer to further increase the stability GM3-NPs in isotonic solution. 10^{11} GM3-NPs in 100 μL PBS or 100 μL PBS as control were intravenously (i.v.) infused to mice by tail vein injection. Six hours postinjection, whole body and *ex vivo* tissue fluorescent intensities were measured by IVIS Spectrum (Xenogen) and quantified as total radiant efficiency (in units of $[p/s]/[\mu W/cm^2]$).

Statistical Analysis. All data are presented as mean ± standard deviation (SD). Data presentation and sample size for statistical analysis of individual experiments are specified in figure captions. Statistical significance of data was determined using two-tail Student's *t*- test. One asterisk (*) indicates significant differences at $p < 0.05$, two asterisks (**) for $p < 0.01$, three asterisks (***) for $p < 0.001$, and four asterisks (****) for $p < 0.0001$. NS was used to indicate nonsignificant differences.

ETHICS STATEMENT

This research has been determined to be exempt by the Institutional Review Board of the Boston University Medical Center, since it does not meet the definition of human subjects research, since all human samples were collected in an anonymous fashion and no identifiable private information was collected.

ASSOCIATED CONTENT

Supporting Information

The Supporting Information is available free of charge online. The Supporting Information is available free of charge at https://pubs.acs.org/doi/10.1021/acsnano.2c06516.

NP number calculation; SEM images of GM3-NPs; activation of WT T cell through CD69 and IL-2 measurement; CD69 measurement with GM3-NPs in absence of CAR ligand; comparison between free vs Raji B/CD169 cell-mediated activation of CAR T cells; scheme of experimental setup used for for Ca^{2+} imaging of Fura-2AM-loaded T cells; Ca^{2+}activity curve of unbound Jurkat T cells and Jurkat WT T cells in contact with GM3-FITC-NP-presenting Raji B/CD169 cells; cell conjugation formation after 2.5 h preincubation of DCs with GM3-NPs; CAR T cell activation after 0−20 h preincubation of DCs with GM3-NPs; in vivo distribution of GM3-NPs after i.v. injection (PDF)

AUTHOR INFORMATION

Corresponding Author

Björn M. Reinhard − *Departments of Chemistry and The Photonics Center, Boston University, Boston, Massachusetts 02215, United States;* orcid.org/0000-0003-2550-5331; Email: bmr@bu.edu

Authors

Han Zang − *Departments of Chemistry and The Photonics Center, Boston University, Boston, Massachusetts 02215, United States;* orcid.org/0000-0002-7192-9605

Menna Siddiqui − *Department of Biomedical Engineering and Biological Design Center, Boston University, Boston, Massachusetts 02215, United States;* orcid.org/0000-0001-5183-1777

Suryaram Gummuluru − *Department of Microbiology, Boston University School of Medicine, Boston, Massachusetts 02118, United States*

Wilson W. Wong − *Department of Biomedical Engineering and Biological Design Center, Boston University, Boston, Massachusetts 02215, United States;* orcid.org/0000-0001-8394-889X

Complete contact information is available at: https://pubs.acs.org/10.1021/acsnano.2c06516

Author Contributions

B.M.R., S.G., W.W.W. and H.Z. conceived the project. H.Z. designed and performed experiments, analyzed the data, and generated figures. M.S. designed and generated genetic constructs, performed Jurkat T cell and primary T cell transduction and helped with cell activation and exhaustion experiments. H.Z. and B.M.R. wrote the manuscript with input from M.S., S.G. and W.W.W. All authors discussed the results and contributed to the manuscript.

Notes

The authors declare the following competing financial interest(s): B.M.R. and S.G. hold patents for GM3 functionalized nanoparticles.

ACKNOWLEDGMENTS

We thank Sarah B. Nodder, Hisashi Akiyama, Andres Quinones and Chelsey Skeete for providing $CD14^+$ monocytes and reagents, Jacob L. Berrigan and Josiane Fofana for providing Raji B cells and Raji B/CD169 cells, and Yuanqing Gu for assistance with ELISA and DLS measurements. Confocal microscopy research reported in this publication was supported by the Boston University Micro and Nano Imaging Facility and the Office of the Director, National Institutes of Health of the National Institutes of Health, under Award No. S10OD024993. B.M.R. acknowledges support from the NIH through Grant Nos. R01GM142012, R01CA138509, R01AI132111. S.G. acknowledges support from the NIH through Grant Nos. R01GM142012, R01AI132111 and R01AI38960. W.W.W. acknowledges support from the NIH,

through Grant Nos. U01CA265713 and R01DK132576. The content is solely the responsibility of the authors and does not necessarily represent the official views of the National Institute of Health.

REFERENCES

(1) Bagley, S. J.; O'Rourke, D. M. Clinical Investigation of CAR T Cells for Solid Tumors: Lessons Learned and Future Directions. *Pharmacol. Ther.* **2020**, *205*, 107419.
(2) Ma, L.; Dichwalkar, T.; Chang, J. Y. H.; Cossette, B.; Garafola, D.; Zhang, A. Q.; Fichter, M.; Wang, C.; Liang, S.; Silva, M.; et al. Enhanced CAR−T Cell Activity against Solid Tumors by Vaccine Boosting through the Chimeric Receptor. *Science* **2019**, *365*, 162−168.
(3) Nakamura, K.; Yagyu, S.; Hirota, S.; Tomida, A.; Kondo, M.; Shigeura, T.; Hasegawa, A.; Tanaka, M.; Nakazawa, Y. Autologous Antigen-Presenting Cells Efficiently Expand PiggyBac Transposon CAR-T Cells with Predominant Memory Phenotype. *Mol. Ther. Methods Clin. Dev.* **2021**, *21*, 315−324.
(4) Xiong, W.; Chen, Y.; Kang, X.; Chen, Z.; Zheng, P.; Hsu, Y. H.; Jang, J. H.; Qin, L.; Liu, H.; Dotti, G.; Liu, D. Immunological Synapse Predicts Effectiveness of Chimeric Antigen Receptor Cells. *Mol. Ther.* **2018**, *26*, 963−975.
(5) Lindner, S. E.; Johnson, S. M.; Brown, C. E.; Wang, L. D. Chimeric Antigen Receptor Signaling: Functional Consequences and Design Implications. *Sci. Adv.* **2020**, *6*, eaaz3223.
(6) Gong, N.; Sheppard, N. C.; Billingsley, M. M.; June, C. H.; Mitchell, M. J. Nanomaterials for T-Cell Cancer Immunotherapy. *Nat. Nanotechnol.* **2021**, *16*, 25−36.
(7) Toy, R.; Roy, K. Engineering Nanoparticles to Overcome Barriers to Immunotherapy. *Bioeng. Transl. Med.* **2016**, *1* (1), 47−62.
(8) Schudel, A.; Francis, D. M.; Thomas, S. N. Material Design for Lymph Node Drug Delivery. *Nat. Rev. Mater.* **2019**, *4*, 415−428.
(9) Manolova, V.; Flace, A.; Bauer, M.; Schwarz, K.; Saudan, P.; Bachmann, M. F. Nanoparticles Target Distinct Dendritic Cell Populations According to Their Size. *Eur. J. Immunol.* **2008**, *38*, 1404−1413.
(10) Grabowska, J.; Lopez-Venegas, M. A.; Affandi, A. J.; den Haan, J. M. M. CD169+ Macrophages Capture and Dendritic Cells Instruct: The Interplay of the Gatekeeper and the General of the Immune System. *Front. Immunol.* **2018**, *9*, 2472.
(11) Villani, A. C.; Satija, R.; Reynolds, G.; Sarkizova, S.; Shekhar, K.; Fletcher, J.; Griesbeck, M.; Butler, A.; Zheng, S.; Lazo, S.; et al. Single-Cell RNA-Seq Reveals New Types of Human Blood Dendritic Cells, Monocytes, and Progenitors. *Science* **2017**, *356*, eaah4573.
(12) Martinez-Pomares, L.; Gordon, S. CD169+ Macrophages at the Crossroads of Antigen Presentation. *Trends Immunol.* **2012**, *33*, 66−70.
(13) Affandi, A. J.; Grabowska, J.; Olesek, K.; Lopez Venegas, M.; Barbaria, A.; Rodríguez, E.; Mulder, P. P. G.; Pijffers, H. J.; Ambrosini, M.; Kalay, H.; O'Toole, T.; Zwart, E. S.; Kazemier, G.; Nazmi, K.; Bikker, F. J.; Stöckl, J.; van den Eertwegh, A. J. M.; de Gruijl, T. D.; Storm, G.; van Kooyk, Y.; den Haan, J. M. M. Selective Tumor Antigen Vaccine Delivery to Human CD169+ Antigen-Presenting Cells Using Ganglioside-Liposomes. *Proc. Natl. Acad. Sci. U.S.A.* **2020**, *117*, 27528−27539.
(14) Crocker, P. R.; Paulson, J. C.; Varki, A. Siglecs and Their Roles in the Immune System. *Nat. Rev. Immunol.* **2007**, *7*, 255−266.
(15) Grabowska, J.; Affandi, A. J.; van Dinther, D.; Nijen Twilhaar, M. K.; Olesek, K.; Hoogterp, L.; Ambrosini, M.; Heijnen, D. A. M.; Klaase, L.; Hidalgo, A.; Asano, K.; Crocker, P. R.; Storm, G.; van Kooyk, Y.; den Haan, J. M. M. Liposome Induction of CD8+ T Cell Responses Depends on CD169+ Macrophages and Batf3-Dependent Dendritic Cells and Is Enhanced by GM3 Inclusion. *J. Controlled Release* **2021**, *331*, 309−320.
(16) Grabowska, J.; Stolk, D. A.; Nijen Twilhaar, M. K.; Ambrosini, M.; Storm, G.; van der Vliet, H. J.; de Gruijl, T. D.; van Kooyk, Y.; den Haan, J. M. M. Liposomal Nanovaccine Containing α-Galactosylceramide and Ganglioside GM3 Stimulates Robust CD8+ T Cell Responses via CD169+ Macrophages and CDC1. *Vaccines* **2021**, *9*, 56.
(17) Kawasaki, N.; Vela, J. L.; Nycholat, C. M.; Rademacher, C.; Khurana, A.; van Rooijen, N.; Crocker, P. R.; Kronenberg, M.; Paulson, J. C. Targeted Delivery of Lipid Antigen to Macrophages via the CD169/Sialoadhesin Endocytic Pathway Induces Robust Invariant Natural Killer T Cell Activation. *Proc. Natl. Acad. Sci. U.S.A.* **2013**, *110*, 7826−7831.
(18) Edgar, L. J.; Kawasaki, N.; Nycholat, C. M.; Paulson, J. C. Targeted Delivery of Antigen to Activated CD169+ Macrophages Induces Bias for Expansion of CD8+ T Cells. *Cell Chem. Biol.* **2019**, *26*, 131−136.
(19) Benne, N.; van Duijn, J.; Kuiper, J.; Jiskoot, W.; Slütter, B. Orchestrating Immune Responses: How Size, Shape and Rigidity Affect the Immunogenicity of Particulate Vaccines. *J. Controlled Release* **2016**, *234*, 124−134.
(20) Zhao, J.; Stenzel, M. H. Entry of Nanoparticles into Cells: The Importance of Nanoparticle Properties. *Polym. Chem.* **2018**, *9*, 259−272.
(21) Zhu, M.; Nie, G.; Meng, H.; Xia, T.; Nel, A.; Zhao, Y. Physicochemical Properties Determine Nanomaterial Cellular Uptake, Transport, and Fate. *Acc. Chem. Res.* **2013**, *46*, 622−631.
(22) Izquierdo-Useros, N.; Lorizate, M.; McLaren, P. J.; Telenti, A.; Kräusslich, H. G.; Martinez-Picado, J. HIV-1 Capture and Transmission by Dendritic Cells: The Role of Viral Glycolipids and the Cellular Receptor Siglec-1. *PLoS Pathog.* **2014**, *10*, e1004146.
(23) Puryear, W. B.; Akiyama, H.; Geer, S. D.; Ramirez, N. P.; Yu, X.; Reinhard, B. M.; Gummuluru, S. Interferon-Inducible Mechanism of Dendritic Cell-Mediated HIV-1 Dissemination Is Dependent on Siglec-1/CD169. *PLoS Pathog.* **2013**, *9*, e1003291.
(24) Deneka, M.; Pelchen-Matthews, A.; Byland, R.; Ruiz-Mateos, E.; Marsh, M. In Macrophages, HIV-1 Assembles into an Intracellular Plasma Membrane Domain Containing the Tetraspanins CD81, CD9, and CD53. *J. Cell Biol.* **2007**, *177*, 329−341.
(25) Yu, H. J.; Reuter, M. A.; McDonald, D. HIV Traffics through a Specialized, Surface-Accessible Intracellular Compartment during Trans-Infection of T Cells by Mature Dendritic Cells. *PLoS Pathog.* **2008**, *4*, e1000134.
(26) Garcia, E.; Pion, M.; Pelchen-Matthews, A.; Collinson, L.; Arrighi, J. F.; Blot, G.; Leuba, F.; Escola, J. M.; Demaurex, N.; Marsh, M.; Piguet, V. HIV-1 Trafficking to the Dendritic Cell−T-Cell Infectious Synapse Uses a Pathway of Tetraspanin Sorting to the Immunological Synapse. *Traffic* **2005**, *6*, 488−501.
(27) McDonald, D.; Wu, L.; Bohks, S. M.; KewalRamani, V. N.; Unutmaz, D.; Hope, T. J. Recruitment of HIV and Its Receptors to Dendritic Cell-T Cell Junctions. *Science* **2003**, *300*, 1295−1297.
(28) Izquierdo-Useros, N.; Blanco, J.; Erkizia, I.; Fernández-Figueras, M. T.; Borràs, F. E.; Naranjo-Gómez, M.; Bofill, M.; Ruiz, L.; Clotet, B.; Martinez-Picado, J. Maturation of Blood-Derived Dendritic Cells Enhances Human Immunodeficiency Virus Type 1 Capture and Transmission. *J. Virol.* **2007**, *81*, 7559−7570.
(29) Hammonds, J. E.; Beeman, N.; Ding, L.; Takushi, S.; Francis, A. C.; Wang, J. J.; Melikyan, G. B.; Spearman, P. Siglec-1 Initiates Formation of the Virus-Containing Compartment and Enhances Macrophage-to-T Cell Transmission of HIV-1. *PLoS Pathog.* **2017**, *13*, e1006181.
(30) Akiyama, H.; Ramirez, N. G. P.; Gudheti, M. v.; Gummuluru, S. CD169-Mediated Trafficking of HIV to Plasma Membrane Invaginations in Dendritic Cells Attenuates Efficacy of Anti-Gp120 Broadly Neutralizing Antibodies. *PLoS Pathog.* **2015**, *11*, e1004751.
(31) Yu, X.; Feizpour, A.; Ramirez, N. G. P.; Wu, L.; Akiyama, H.; Xu, F.; Gummuluru, S.; Reinhard, B. M. Glycosphingolipid-Functionalized Nanoparticles Recapitulate CD169-Dependent HIV-1 Uptake and Trafficking in Dendritic Cells. *Nat. Commun.* **2014**, *5*, 1−12.
(32) Xu, F.; Bandara, A.; Akiyama, H.; Eshaghi, B.; Stelter, D.; Keyes, T.; Straub, J. E.; Gummuluru, S.; Reinhard, B. M. Membrane-Wrapped Nanoparticles Probe Divergent Roles of GM3 and

https://doi.org/10.1021/acsnano.2c06516
ACS Nano XXXX, XXX, XXX−XXX

Phosphatidylserine in Lipid-Mediated Viral Entry Pathways. *Proc. Natl. Acad. Sci. U.S.A.* **2018**, *115*, E9041−E9050.
(33) Eshaghi, B.; Alsharif, N.; An, X.; Akiyama, H.; Brown, K. A.; Gummuluru, S.; Reinhard, B. M. Stiffness of HIV-1 Mimicking Polymer Nanoparticles Modulates Ganglioside-Mediated Cellular Uptake and Trafficking. *Adv. Sci.* **2020**, *7*, 2000649.
(34) Eshaghi, B.; Fofana, J.; Nodder, S. B.; Gummuluru, S.; Reinhard, B. M. Virus-Mimicking Polymer Nanoparticles Targeting CD169+ Macrophages as Long-Acting Nanocarriers for Combination Antiretrovirals. *ACS Appl. Mater. Interfaces* **2022**, *14*, 2488−2500.
(35) Xu, F.; Reiser, M.; Yu, X.; Gummuluru, S.; Wetzler, L.; Reinhard, B. M. Lipid-Mediated Targeting with Membrane-Wrapped Nanoparticles in the Presence of Corona Formation. *ACS Nano* **2016**, *10*, 1189−1200.
(36) Yu, X.; Xu, F.; Ramirez, N. G. P.; Kijewski, S. D. G.; Akiyama, H.; Gummuluru, S.; Reinhard, B. M. Dressing up Nanoparticles: A Membrane Wrap to Induce Formation of the Virological Synapse. *ACS Nano* **2015**, *9*, 4182−4192.
(37) Eggermont, L. J.; Paulis, L. E.; Tel, J.; Figdor, C. G. Towards Efficient Cancer Immunotherapy: Advances in Developing Artificial Antigen-Presenting Cells. *Trends Biotechnol.* **2014**, *32*, 456−465.
(38) Isser, A.; Livingston, N. K.; Schneck, J. P. Biomaterials to Enhance Antigen-Specific T Cell Expansion for Cancer Immunotherapy. *Biomaterials* **2021**, *268*, 120584.
(39) Perica, K.; Kosmides, A. K.; Schneck, J. P. Linking Form to Function: Biophysical Aspects of Artificial Antigen Presenting Cell Design. *Biochim. Biophys. Acta* **2015**, *1853*, 781−790.
(40) Cheung, A. S.; Zhang, D. K. Y.; Koshy, S. T.; Mooney, D. J. Scaffolds That Mimic Antigen-Presenting Cells Enable Ex Vivo Expansion of Primary T Cells. *Nat. Biotechnol.* **2018**, *36*, 160−169.
(41) Perica, K.; de León Medero, A.; Durai, M.; Chiu, Y. L.; Bieler, J. G.; Sibener, L.; Niemöller, M.; Assenmacher, M.; Richter, A.; Edidin, M.; Oelke, M.; Schneck, J. Nanoscale Artificial Antigen Presenting Cells for T Cell Immunotherapy. *Nanomedicine* **2014**, *10*, 119−129.
(42) Perica, K.; Tu, A.; Richter, A.; Bieler, J. G.; Edidin, M.; Schneck, J. P. Magnetic Field-Induced t Cell Receptor Clustering by Nanoparticles Enhances t Cell Activation and Stimulates Antitumor Activity. *ACS Nano* **2014**, *8*, 2252−2260.
(43) Jiang, Y.; Krishnan, N.; Zhou, J.; Chekuri, S.; Wei, X.; Kroll, A. v.; Yu, C. L.; Duan, Y.; Gao, W.; Fang, R. H.; Zhang, L. Engineered Cell-Membrane-Coated Nanoparticles Directly Present Tumor Antigens to Promote Anticancer Immunity. *Adv. Mater.* **2020**, *32*, e2001808.
(44) Sunshine, J. C.; Perica, K.; Schneck, J. P.; Green, J. J. Particle Shape Dependence of CD8+ T Cell Activation by Artificial Antigen Presenting Cells. *Biomaterials* **2014**, *35*, 269−277.
(45) Rhodes, K. R.; Green, J. J. Nanoscale Artificial Antigen Presenting Cells for Cancer Immunotherapy. *Mol. Immunol.* **2018**, *98*, 13−18.
(46) Lewis, R. S. Calcium Oscillations in T-Cells: Mechanisms and Consequences for Gene Expression. *Biochem. Soc. Trans.* **2003**, *31*, 925−929.
(47) Lewis, R. S. Calcium Signaling Mechanisms in T Lymphocytes. *Annu. Rev. Immunol.* **2001**, *19*, 497−521.
(48) James, J. R.; Vale, R. D. Biophysical Mechanism of T-Cell Receptor Triggering in a Reconstituted System. *Nature* **2012**, *487*, 64−69.
(49) Chang, Z. L.; Lorenzini, M. H.; Chen, X.; Tran, U.; Bangayan, N. J.; Chen, Y. Y. Rewiring T-Cell Responses to Soluble Factors with Chimeric Antigen Receptors. *Nat. Chem. Biol.* **2018**, *14*, 317−324.
(50) Lanzavecchia, A.; Sallusto, F. Regulation of T Cell Immunity by Dendritic Cells. *Cell* **2001**, *106*, 263−266.
(51) Sallusto, F.; Lanzavecchia, A. The Instructive Role of Dendritic Cells on T-Cell Responses. *Arthritis Res.* **2002**, *4*, S127−S132.
(52) Guermonprez, P.; Valladeau, J.; Zitvogel, L.; Théry, C.; Amigorena, S. Antigen Presentation and T Cell Stimulation by Dendritic Cells. *Annu. Rev. Immunol.* **2002**, *20*, 621−667.
(53) Izquierdo-Useros, N.; Lorizate, M.; Puertas, M. C.; Rodriguez-Plata, M. T.; Zangger, N.; Erikson, E.; Pino, M.; Erkizia, I.; Glass, B.; Clotet, B.; Keppler, O. T.; Telenti, A.; Kräusslich, H. G.; Martinez-Picado, J. Siglec-1 Is a Novel Dendritic Cell Receptor That Mediates HIV-1 Trans-Infection Through Recognition of Viral Membrane Gangliosides. *PLoS Biol.* **2012**, *10*, e1001448.
(54) Yu, H. J.; Reuter, M. A.; McDonald, D. HIV Traffics through a Specialized, Surface-Accessible Intracellular Compartment during Trans-Infection of T Cells by Mature Dendritic Cells. *PLoS Pathog.* **2008**, *4*, e1000134.
(55) Caruso, H. G.; Tanaka, R.; Liang, J.; Ling, X.; Sabbagh, A.; Henry, V. K.; Collier, T. L.; Heimberger, A. B. Shortened Ex Vivo Manufacturing Time of EGFRvIII-Specific Chimeric Antigen Receptor (CAR) T Cells Reduces Immune Exhaustion and Enhances Antiglioma Therapeutic Function. *J. Neurooncol.* **2019**, *145*, 429−439.
(56) Blumenthal, D.; Burkhardt, J. K. Multiple Actin Networks Coordinate Mechanotransduction at the Immunological Synapse. *J. Cell Biol.* **2020**, *219*, e201911058.
(57) Hammer, J. A.; Wang, J. C.; Saeed, M.; Pedrosa, A. T. Origin, Organization, Dynamics, and Function of Actin and Actomyosin Networks at the T Cell Immunological Synapse. *Annu. Rev. Immunol.* **2019**, *37*, 201−224.
(58) Davenport, A. J.; Cross, R. S.; Watson, K. A.; Liao, Y.; Shi, W.; Prince, H. M.; Beavis, P. A.; Trapani, J. A.; Kershaw, M. H.; Ritchie, D. S.; et al. Chimeric Antigen Receptor T Cells Form Nonclassical and Potent Immune Synapses Driving Rapid Cytotoxicity. *Proc. Natl. Acad. Sci. U.S.A.* **2018**, *115*, E2068−E2076.
(59) Ardeshna, K. M.; Pizzey, A. R.; Devereux, S.; Khwaja, A. The PI3 Kinase, P38 SAP Kinase, and NF-KB Signal Transduction Pathways Are Involved in the Survival and Maturation of Lipopolysaccharide-Stimulated Human Monocyte-Derived Dendritic Cells. *Blood* **2000**, *96*, 1039−1046.
(60) Ma, J. S. Y.; Kim, J. Y.; Kazane, S. A.; Choi, S. H.; Yun, H. Y.; Kim, M. S.; Rodgers, D. T.; Pugh, H. M.; Singer, O.; Sun, S. B.; et al. Versatile Strategy for Controlling the Specificity and Activity of Engineered T Cells. *Proc. Natl. Acad. Sci. U.S.A.* **2016**, *113*, E450−E458.
(61) Zheng, Y.; Nandakumar, K. S.; Cheng, K. Optimization of CAR-T Cell-Based Therapies Using Small-Molecule-Based Safety Switches. *J. Med. Chem.* **2021**, *64*, 9577−9591.
(62) Tamada, K.; Geng, D.; Sakoda, Y.; Bansal, N.; Srivastava, R.; Li, Z.; Davila, E. Redirecting Gene-Modified T Cells toward Various Cancer Types Using Tagged Antibodies. *Clin. Cancer Res.* **2012**, *18*, 6436−6445.
(63) Kim, M. S.; Ma, J. S. Y.; Yun, H.; Cao, Y.; Kim, J. Y.; Chi, V.; Wang, D.; Woods, A.; Sherwood, L.; Caballero, D.; Gonzalez, J.; Schultz, P. G.; Young, T. S.; Kim, C. H. Redirection of Genetically Engineered CAR-T Cells Using Bifunctional Small Molecules. *J. Am. Chem. Soc.* **2015**, *137*, 2832−2835.
(64) Liu, D.; Zhao, J.; Song, Y. Engineering Switchable and Programmable Universal CARs for CAR T Therapy. *J. Hematol. Oncol.* **2019**, *12*, 1−9.
(65) Bragagni, M.; Beneitez, C.; Martín, C.; de La Ossa, D. H. P.; Mura, P. A.; Gil-Alegre, M. E. Selection of PLA Polymers for the Development of Injectable Prilocaine Controlled Release Microparticles: Usefulness of Thermal Analysis. *Int. J. Pharm.* **2013**, *441*, 468−475.
(66) Zhang, L.; Chan, J. M.; Gu, F. X.; Rhee, J. W.; Wang, A. Z.; Radovic-Moreno, A. F.; Alexis, F.; Langer, R.; Farokhzad, O. C. Self-Assembled Lipid-Polymer Hybrid Nanoparticles: A Robust Drug Delivery Platform. *ACS Nano* **2008**, *2*, 1696−1702.

https://doi.org/10.1021/acsnano.2c06516
ACS Nano XXXX, XXX, XXX−XXX